

Softened Spin Waves in Films with Perpendicular Magnetic Anisotropy: Sombbrero-Like Dispersion, Negative Reflection, Bi-, and Trireflection

Nikodem Leśniewski,^{1,2,*} Yuliya S. Dadoenkova,³ Florian F. L. Bentivegna,¹ and Paweł Gruszecki^{2,†}

¹*CNRS, Lab-STICC, UMR 6285, ENIB, 29238 Brest Cedex 3, France*

²*Institute of Spintronics and Quantum Information,
Faculty of Physics, Adam Mickiewicz University,
Uniwersytetu Poznańskiego 2, 61-614 Poznań, Poland*

³*Université Jean Monnet Saint-Etienne, CNRS, Institut d'Optique Graduate School,
Laboratoire Hubert Curien, UMR 5516, 42023 Saint-Etienne, France*

(Dated: February 17, 2025)

We theoretically investigate the effect of perpendicular magnetic anisotropy (PMA) on spin wave (SW) dynamics at low magnetic fields. PMA exerts an in-plane torque on magnetization, counteracting exchange, dipolar, and Zeeman torques, thereby significantly transforming SW dynamics. In ultrathin films, sombrero-like dispersion relation facilitates bireflection and negative reflection of SWs, while in thicker films we demonstrate anti-Larmor precession, cowboy-hat-like dispersion relation, and trireflection of SWs. These results open up new opportunities to explore wave phenomena beyond magnonics.

arXiv:2502.10085v1 [cond-mat.mes-hall] 14 Feb 2025

* nikles@amu.edu.pl

† gruszecki@amu.edu.pl

Introduction— Refraction and specular reflection of light are extensively studied across wave physics, revealing intriguing propagation phenomena. The laws of reflection and refraction were first discovered in 984 by Persian mathematician Ibn Sahl [1], rediscovered by Snellius, and later formalized by Descartes in 1637 [2]. Snell’s law, in its generalized form, states that the tangential component of the wavevector to the interface is conserved during reflection and refraction—a principle known as phase matching. This fundamental rule governs waves in both isotropic and anisotropic media, describing not only electromagnetic waves [3] but also spin waves (SWs) [4–9], which exhibit far more complex and tunable dispersion relationships than light.

Among refraction effects, negative refraction has attracted significant attention in recent decades [10–16]. It is typically achieved via strong anisotropy in the medium [11, 12, 17, 18], photonic metamaterials [10, 14, 16], or specially engineered interfaces (e.g. metasurfaces introducing phase gradients) [19–22]. In contrast to negative refraction and anomalous reflection [23], in negative reflection, the reflected wave appears on the same side of the normal as incident wave. This effect is less explored, with demonstrations limited to specific interface properties [13, 24, 25] or medium anisotropy [12, 26]. Another notable specular effect is *bireflection* [18, 27], akin to birefringence, where an incident wave splits into two reflected waves. However, neither negative reflection nor *bireflection* has been demonstrated in isotropic media at uniform interfaces, without structural modifications such as diffraction gratings or metasurfaces. In this Letter, we describe how negative and multiple reflection, along other remarkable behaviors, can take place for SWs in thin magnetic films with perpendicular magnetic anisotropy.

In magnetic films, perpendicular magnetic anisotropy (PMA) favors the alignment of magnetic moments perpendicular to the film’s surface [28–30] affecting both the static magnetic configuration (e.g. leading to periodic stripe domains at magnetic fields lower than the critical magnetic field H^{cr} [29, 31]) and magnetization dynamics [32–36]. At low magnetic fields above the critical value, in uniformly in-plane magnetized films, PMA creates a local minimum in the dispersion of Damon-Eshbach (DE) SWs [37]. The dynamics of softened SW mode [34] with frequencies approaching zero has been related to the periodicity and spatial distribution of the magnetization texture after the phase transition from uniform to stripe-domain phase in films [38] and stripes [39, 40]. Near this transition at H^{cr} , the softened modes splits into a zero-frequency Goldstone mode and a non-zero-frequency Higgs mode on the low-symmetry side [34]. Although PMA suggests a variety of intriguing phenomena in SW dynamics near the phase transition, the behavior of SWs at low fields just above the H^{cr} remains unexplored.

In this Letter, we investigate the influence of PMA on the dynamics of SWs in the linear regime in uniformly in-plane magnetized thin films at low magnetic fields near the H^{cr} . We demonstrate that PMA significantly modi-

fies the overall torque acting on magnetization, leading to fundamental changes enabling the manifestation of novel phenomena. Our analysis begins with the simpler case of ultrathin films (where SW profiles are uniform through the thickness) and progresses to the more complex scenario of thicker films.

Theoretical description of SWs in an ultrathin film with PMA—In the following, we consider thin magnetic films with surfaces parallel to the xy -plane and exhibiting PMA along the z -axis of a Cartesian system of coordinates. For an ultrathin film uniformly magnetized in-plane along the y -axis by an external field H_0 , the dynamic dipolar magnetic field can be approximated to the form $\mathbf{h}^{\text{d}} = [h_x^{\text{d}}, 0, h_z^{\text{d}}] = [\xi(kd)\sin^2(\theta)m_x, 0, (1 - \xi(kd)m_z)]$, where m_x and m_z are dynamic components of magnetization, d is the film thickness, $\xi(x) = 1 - (1 - e^{-|x|})/|x|$, and θ is the angle of SW propagation with respect to the bias magnetic field [41, 42]. In such a film the linearized Landau-Lifshitz equation (neglecting damping) for magnetization dynamics is given as:

$$\begin{aligned} \partial_t m_x &= \left(\underbrace{\frac{\tau_x^0}{M_s}}_{\frac{H_0}{M_s}} + \underbrace{\frac{\tau_x^{\text{ex}}}{cm_z}}_{+l_{\text{ex}}^2 k^2} + \underbrace{\frac{\tau_x^{\text{d}}}{cm_z}}_{+h_z^{\text{d}}} - \underbrace{\frac{\tau_x^{\text{PMA}}}{cm_z}}_{-Q} \right) cm_z, \\ \partial_t m_z &= \left(-\underbrace{\frac{H_0}{M_s}}_{\frac{\tau_z^0}{cm_x}} - \underbrace{l_{\text{ex}}^2 k^2}_{\frac{\tau_z^{\text{ex}}}{cm_x}} - \underbrace{h_x^{\text{d}}}_{\frac{\tau_z^{\text{d}}}{cm_x}} \right) cm_x \end{aligned} \quad (1)$$

where M_s is the saturation magnetization, $l_{\text{ex}} = \sqrt{A/(\frac{1}{2}\mu_0 M_s^2)}$ is the exchange length and A is the exchange constant, μ_0 is the permeability of vacuum, k is the wavenumber, $Q = K_{\text{u}}/(\frac{1}{2}\mu_0 M_s^2)$ is the reduced perpendicular magnetic anisotropy constant (with K_{u} is uniaxial anisotropy constant), and $c = |\gamma|\mu_0 M_s$ with γ is the gyromagnetic ratio. The sign of c defines the sense of precession of the ferromagnetic resonance (FMR) mode, which is the Larmor precession direction.

Eq. 1 can be written as $[\partial_t m_x, \partial_t m_z] = [\tau_x^{\text{eff}}, \tau_z^{\text{eff}}]$, where τ_x^{eff} and τ_z^{eff} are the x - and z -components of the effective torque acting on magnetization. The total torque is the sum of several terms: $\tau^{\text{eff}} = \tau^0 + \tau^{\text{ex}} + \tau^{\text{d}} + \tau^{\text{PMA}}$ representing torques due to the external (Zeeman), exchange, dipole, and PMA fields, respectively (see definition of torques in Appendix A. PMA torque $\tau^{\text{PMA}} = c[-Qm_z, 0]$ has only the x -component and acts opposite to the other torques, squeezing the precession orbit along the x -axis. For $Q > H_0/M_s + l_{\text{ex}}^2 k^2 + h_z^{\text{d}}$ (in ultrathin films $h_z^{\text{d}} > 0$), the magnetic moment precession around the y -axis is expected to reverse. However, solving Eq. (1) for this condition, the time dependence of $m_{x,z}$ is not harmonic ($\propto e^{-i\omega t}$) but instead grows unbounded over time (see Supplementary Material (SM)). This occurs because the assumed uniform magnetic configuration along the y -axis is unstable, leading to a phase transition to an out-of-plane stripe-domain configuration [38]. We will revisit the reversal of the precession direction later in the

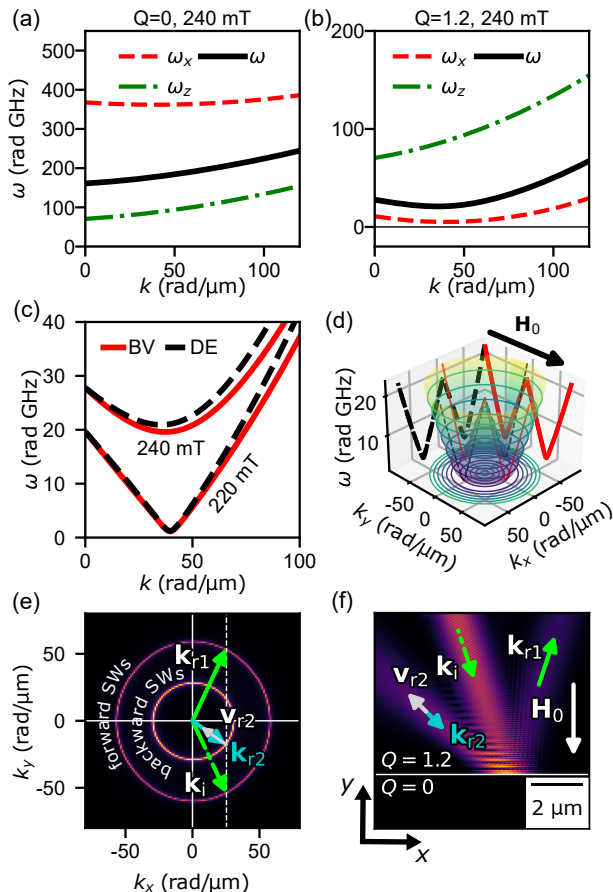


FIG. 1. (a)-(b) SW dispersion relations for 2-nm-thick CoFeB film with $Q = 0$ (a) and $Q = 1.2$ (b): $\omega = \sqrt{\omega_x \omega_z}$ (black), ω_x (red, Eq. (A7)), and ω_z (green, Eq. (A8)). (c) Dispersion relations for external magnetic fields of 220 mT (lower pair) and 240 mT (upper pair) in both BV (red) and DE (dashed black) geometries. (d) Dispersion relations as a function of k_x and k_y ; red and black lines show the cross-sections for $k_x = 0$ (BV) and $k_y = 0$ (DE), with circles indicating exemplary IFCs for different frequencies. (e) IFC at 1.5 GHz computed using MUMAX3, showing incident and reflected wavevectors \mathbf{k}_i , \mathbf{k}_{r1} , and \mathbf{k}_{r2} ; the group velocity direction for \mathbf{k}_{r2} is indicated by the white arrow. (f) Micromagnetic simulation of the reflection of an SW beam in a 2 nm CoFeB film, incident at a 25° angle on an interface separating regions with different Q values. Wavevectors (parallel to phase velocities) and group velocity directions from (e) are marked by arrows.

manuscript.

Ultrathin films with PMA— The dispersion relations $\omega = \sqrt{\omega_x \omega_z}$ (see Appendix B for details) for CoFeB ($M_s = 1344$ kA/m, $A = 13.6$ pJ/m) with $Q = 0$ and $Q = 1.2$ are shown in Fig. 1 (a) and (b). ω_z increases monotonically, while ω_x exhibits a minimum corresponding to the k -vector where exchange interactions start to dominate over dipolar interactions. The values of Q and H_0 shift ω_z up or down. For sufficiently high Q and small H_0 , the ω_x dependence can shift enough to introduce a minimum in ω , with PMA playing a key role in this transition. Further details on the conditions for this minimum are provided in the SM. Figure 1(c) shows dis-

persion relations for a system with $Q = 1.2$ along two orthogonal propagation directions (BV and DE configurations) at magnetic fields of 220 mT and 240 mT. A small decrease in the field significantly affects the dispersion: at 240 mT, the DE and BV SW minima are about 20 rad GHz (with the BV slightly lower). At 220 mT, the minimum deepens approaching zero frequency, with DE and BV dispersions overlapping for $k < 60$ rad/ μm .

The dispersion relation $\omega(k_x, k_y)$ shown in Fig. 1(d) for 220 mT resembles the sombrero potential appearing in various physical systems [43]. It features two circular isofrequency contours (IFCs) below the FMR frequency $f(k=0)$, an outer contour for forward SWs, where group and phase velocities are parallel, and an inner contour for backward SWs, where they are antiparallel. Fig. 1(e) shows exemplary contours for $f = 1.5$ GHz and 380 mT, computed using MUMAX3 (see SM for details) [44]. The dispersion relation with minimum extending for all angles of propagation opens new avenues in nonlinear physics, e.g., magnon Bose-Einstein condensation [45].

Two IFCs imply that if the tangential wavevector, component k_x of the incident wavevector, is smaller than the inner contour radius, two reflected waves (one forward and one backward) can form, as shown in Fig. 1(e). The wavevectors of the incident wave (\mathbf{k}_i) and the reflected SWs (\mathbf{k}_{r1} for the forward SW, and \mathbf{k}_{r2} for the backward SW) are marked. The forward wave \mathbf{k}_{r1} follows a specular reflection rule, whereas the second reflected wave (\mathbf{k}_{r2}) exhibits unique properties. First, its phase and group velocities are opposite, although it is not a classical backward volume magnetostatic mode (with $k_x = 0$). Second, the energy of the reflected waves (associated with the group velocity direction) must flow outwards from the edge, with the y -component of the group velocity being positive ($v_{g,y} > 0$). Consequently, the wavevector of the backward SW lies in the same quadrant of wavevector space as the incident SW.

To verify this, we performed micromagnetic simulations (see Fig. 1(f); see SM for details). In the simulations, a SW beam at a frequency of 1.5 GHz is incident at a 25° angle on a sharp interface separating two uniform regions. The first, where the SWs are excited has PMA ($Q = 1.2$), and the second has no PMA ($Q = 0$). The magnetic field is applied along the y -axis. The simulation results reveal two reflected beams, i.e., a *bireflection*. The first beam, with wavevector \mathbf{k}_{r1} , is reflected under the same angle as the angle of incidence. The second beam, with wavevector \mathbf{k}_{r2} , has a negative angle of reflection (is located on the same side of the normal as the incident wave), and its group velocity is antiparallel to the wavevector. This behavior, previously unobserved in optics, results in negative reflection in an isotropic medium, where the reflection angle is negative. While negative reflection has been reported for light [24], polaritons [12], and acoustic waves [13], these cases relied on strong anisotropy in the dispersion relation or on nonuniform interfaces (e.g., diffraction gratings). To our knowledge, negative reflection in a uniform isotropic medium

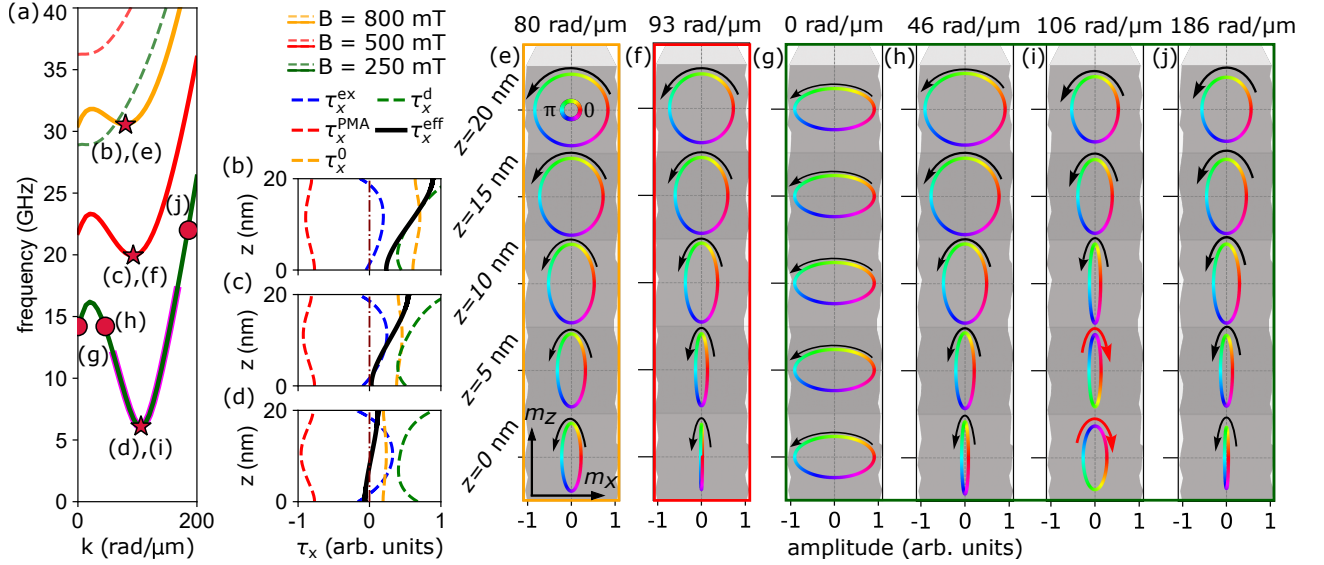


FIG. 2. (a) Dispersion relations for the first (bold solid lines) and second (narrow dashed lines) bands of a 20 nm CoFeB film with $Q = 0.6$ at 250 mT (green), 500 mT (red), and 800 mT (orange). Letters (b)-(j) correspond to k and field values marked by dots and stars in (a). The thick magenta line for 250 mT shows the range where anti-Larmor precession occurs. (b)-(d) x -component of the torque (τ_x) across the film thickness for wavevectors marked by stars in (a), corresponding to wavevectors and fields of 80 $\text{rad}/\mu\text{m}$ at 800 mT, 93 $\text{rad}/\mu\text{m}$ at 500 mT, and 106 $\text{rad}/\mu\text{m}$ at 250 mT. The dashed blue, green, red, and orange lines show the exchange, dipolar, PMA, and Zeeman components of τ_x , respectively, with the solid black line indicating the effective torque. (e)-(j) Precession orbits of the magnetic moments at $z = 0, 5, 10, 15,$ and 20 nm. Colors represent phase, while black and red arrows indicate Larmor and anti-Larmor precession, respectively. Panel (e) corresponds to 800 mT, (f) to 500 mT, and (g)-(j) to 250 mT. k values are shown at the top of each subplot. See SM for the animated version of (e)-(j).

at a sharp interface has never been demonstrated for any type of wave. Due to isotropic dispersion, this effect occurs at any field-wavevector angle, unlike in PMA-free layers, where dispersion is highly anisotropic.

Thicker films with PMA—Let us test the hypothesis that increasing the film thickness (which enhances dipole interactions) can lead to anti-Larmor precession. In thicker films, the SW amplitude and dipolar field vary through the film's thickness, along the z -axis, making the previously used dipole field formula invalid. To address this, we use the finite-element method (FEM) in COMSOL MULTIPHYSICS [46–48] to solve Eq. (1), coupled with Gauss's equation for the dipolar field, and compute the dispersion relation and mode profiles for SWs in a 20 nm thick CoFeB film ($Q = 0.6$) (see details in SM). Results for three magnetic field values (800, 500, and 250 mT) are shown in Fig. 2(a). The dispersions are nonmonotonic, exhibiting successive positive, negative, and positive slopes, similar to experimental observations [34, 37, 49]. The initial positive slope results from stronger dipole interactions in thicker films compared to the ultrathin case (cf. Fig. 1(c)). As the field decreases, the minimum becomes more pronounced and shifts to larger wavevectors [38], resembling the behavior observed in ultrathin films (Fig. 1(c)).

Fig. 2(e-j) depicts the precession orbits across the thickness for several different cases of wavevector and magnetic field values (marked by the labels in Fig. 2(a)). For all cases except the FMR mode ($k = 0$), the precession ellipticity varies with the z -coordinate. As z decreases, the precession orbit becomes more polarized

along the z -axis since the amplitude of m_x is reduced. The key result is shown in Fig. 2(i) with precession orbits for 250 mT and wavevector from the dispersion relation minimum ($k_x = 106 \text{ rad}/\mu\text{m}$). The precession direction of the magnetic moments is reversed at the bottom of the film, indicating anti-Larmor precession. This effect occurs only for wavevectors near the minimum of the dispersion relation, as marked in Fig. 2(a). Anti-Larmor precession at a surface was predicted theoretically [50, 51]. In Ref. [52], these modes were termed heterosymmetric SWs (due to different symmetry of m_x and m_z) and attributed to hybridization between the fundamental and first perpendicular standing SWs [52, 53]. In our system, the frequency difference between the first and second SW bands is on the order of dozens of GHz, i.e. 14.7 GHz at $k = 0$, and for wavevectors exhibiting anti-Larmor precession above 20 GHz (27 GHz at 100 $\text{rad}/\mu\text{m}$). It indicates the PMA origin of these modes.

To explain the heterosymmetric nature of the modes and confirm their PMA origin, we analyze the x -component of torque terms from Eq. (1) at the dispersion minimum for fields of 800, 500, and 250 mT, shown in Fig. 2(b-d). A detailed analysis of x - and z -components is in the SM. The PMA torque τ_x^{PMA} has a sign opposite to that of the other torques. Due to the varying strength of dipolar interactions across the film, the dipolar torque τ_x^{d} is stronger at the top, leading to a larger τ_x^{eff} there. As the bias field decreases, the Zeeman torque τ_x^{Zeeman} weakens, causing τ_x^{eff} to decrease. At the field 250 mT, τ_x^{eff} crosses zero, reversing the precession direction. Note that τ_z^{eff} does not cross zero, as shown in the SM.

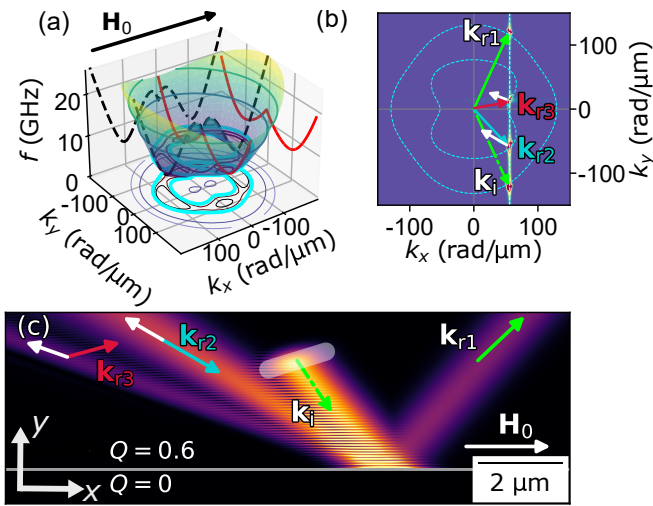


FIG. 3. (a) Dispersion relation $f(k_x, k_y)$ for a 20 nm CoFeB film ($Q = 0.6$, $H_0 = 250$ mT), calculated using FEM. The red and black curves show cross-sections for $k_x = 0$ (BV) and $k_y = 0$ (DE) configurations. Circles at the bottom represent IFCs at different frequencies, with the 9 GHz contour highlighted in cyan. (b) IFC at 9 GHz (cyan dashed lines), extracted from (a). The colormap in the background (representing the 2D Fourier transform of (c)) shows small bright spots (see SM for a larger version of the colormap). (c) Reflection of an SW beam in a 2 nm CoFeB film, incident at 24.5° from the $Q = 0.6$ region to the $Q = 0$ region at a sharp interface. The semi-transparent white area marks the excitation region. Wavevector directions in (b) and (c) are shown by green (\mathbf{k}_i , \mathbf{k}_{r1}), cyan (\mathbf{k}_{r2}), and red (\mathbf{k}_{r3}) arrows, with white arrows indicating group velocity directions for \mathbf{k}_{r2} and \mathbf{k}_{r3} .

This clearly indicates that we have identified a new class of heterosymmetric SWs, where anti-Larmor precession at the bottom surface results from PMA-induced torque and dipolar field nonuniform through the thickness, typical for DE SWs in thicker films.

Finally, we examine how increased dipole interactions, resulting from greater film thickness, affect the sombrero-like shape of the dispersion relation. As shown in Fig. 3(a), the dispersion for a 20 nm thick CoFeB film is anisotropic, transitioning from a sombrero to a cowboy-hat shape. This change introduces a greater variety of IFCs (shown on the bottom surface of the plot), including frequencies with two closed contours (i.e., 9 GHz, cyan lines) or even four closed contours (i.e., 7.9 GHz, black lines). More IFCs can be found in Appendix C. Focusing on the 9 GHz IFC in Fig. 3(b), we observe that the outer and inner contours correspond to forward (group velocity directed away from the IFC center) and backward (group velocity directed towards the IFC center) SWs. As these contours are no longer circular, the direction of the group velocity can differ significantly from the phase velocity, unlike in ultrathin layers where they are either parallel or antiparallel. Even flat segments are visible, essential for observing caustics. [54, 55]. As an example, let us demonstrate *trireflection* of SWs (a scenario in which we observe three reflected waves with different wavevectors). As presented in Fig. 3(b), this can, for

instance, be achieved with an incident wavevector \mathbf{k}_i corresponding to the angle of incidence 24.5° for which we can find three wavevectors for the reflected waves (with the same value of k_x and positive y -component of the group velocity $v_{g,y} > 0$).

To verify this prediction, we perform micromagnetic simulations with an oblique incident SW beam (see Fig. 3(c) and details of simulations in SM). Three reflected SW beams are observed: one with the same angle as the incident wave, and two with negative reflection angles (-60° and -70.7°). The two-dimensional Fourier transform of this result, shown in the background of Fig. 3(b), reveals four bright spots on the IFC, corresponding to the same k_x value and the predicted wavevectors. The third reflected wave, \mathbf{k}_{r3} , lies on the inner IFC in the same quadrant as the ordinary reflected wave (\mathbf{k}_{r1}) on the forward IFC. This wave, located in the backward IFC, can propagate outwards from the interface due to the anisotropic IFC, allowing the group velocity to be directed outward the boundary ($v_{g,y} > 0$), with the group velocity nearly perpendicular to the wavevector. Additionally, the third beam is narrower and exhibits almost no spreading, characteristic of caustic-like beams whose wavevectors lie on flat segments of the IFC (as in the case of \mathbf{k}_{r3}). To the best of our knowledge, this is the first numerical observation of three reflected waves resulting from reflection at a uniform plane boundary between two media, without nanostructuring, complex interface engineering, or modulating the beam itself. This finding may provide new insights into wave propagation and applications involving multiple-wave interactions at interfaces.

Summary and outlook— We have theoretically investigated the impact of PMA on SW dynamics in uniformly in-plane magnetized thin films at low magnetic fields, where Zeeman interactions are negligible compared to PMA. We show that, due to the in-plane torque exerted by PMA on the magnetization, which tends to reverse the precession direction of the magnetic moments, anti-Larmor precession (for heterosymmetric modes) can be achieved under specific conditions. Furthermore, PMA significantly modifies the dispersion relation. For ultrathin films, the dispersion exhibits an isotropic sombrero-like shape, whereas, for thicker films, it becomes anisotropic, resembling a cowboy-hat-like form. In both cases, frequency ranges exist where both forward and backward SWs are present across all directions of propagation. This presents unique opportunities to explore new wave phenomena, extending beyond magnonics into broader wave physics. This finding highlights the potential to engineer dispersion relations through the interplay of PMA and magnetic-field-induced torques, enabling novel phenomena such as the reflection of wave beams into two or three beams, reflected with both positive and negative angles of reflection. The dynamics of softened SW modes near the dispersion minimum in PMA films shows great promise for nonlinear physics applications since the response of softened SWs on microwave field is enhanced [38].

Acknowledgments—The research leading to these results has received funding from the National Science Centre of Poland, project no. 2019/35/D/ST3/03729 and

the Regional Council of Brittany (France) and ENIB, project AMOSPIN. The authors thank M. Krawczyk and K. Szulc for valuable discussions.

-
- [1] R. Rashed, *Géométrie et dioptrique au Xe siècle: Ibn Sahl, al-Quhi et Ibn al-Haytham* (Les Belles Lettres, Paris, 1993).
- [2] R. Descartes, *Discours de la méthode pour bien conduire sa raison, et chercher la vérité dans les sciences* (Jan Maire, Leiden, Netherlands, 1637) contains the law of refraction.
- [3] E. Hecht, *Optics*, 5th ed. (Pearson, 2016).
- [4] P. Gruszecki, J. Romero-Vivas, Y. S. Dadoenkova, N. Dadoenkova, I. Lyubchanskii, and M. Krawczyk, Goos-Hänchen effect and bending of spin wave beams in thin magnetic films, *Applied Physics Letters* **105** (2014).
- [5] J. Stigloher, M. Decker, H. S. Körner, K. Tanabe, T. Moriyama, T. Taniguchi, H. Hata, M. Madami, G. Gubbiotti, K. Kobayashi, *et al.*, Snell's law for spin waves, *Physical Review Letters* **117**, 037204 (2016).
- [6] W. Yu, J. Lan, R. Wu, and J. Xiao, Magnetic Snell's law and spin-wave fiber with Dzyaloshinskii-Moriya interaction, *Physical Review B* **94**, 140410 (2016).
- [7] J. Mulkers, B. Van Waeyenberge, and M. V. Milošević, Tunable Snell's law for spin waves in heterochiral magnetic films, *Physical Review B* **97**, 104422 (2018).
- [8] P. Gruszecki and M. Krawczyk, Spin-wave beam propagation in ferromagnetic thin films with graded refractive index: Mirage effect and prospective applications, *Physical Review B* **97**, 094424 (2018).
- [9] W. Zhu, H. Qin, L. Flajšman, T. Taniyama, and S. Van Dijken, Zero-field routing of spin waves in a multiferroic heterostructure, *Applied Physics Letters* **120** (2022).
- [10] A. Poddubny, I. Iorsh, P. Belov, and Y. Kivshar, Hyperbolic metamaterials, *Nature Photonics* **7**, 948–957 (2013).
- [11] R. Macêdo and T. Dumelow, Tunable all-angle negative refraction using antiferromagnets, *Physical Review B* **89**, 10.1103/physrevb.89.035135 (2014).
- [12] T. Zhang, C. Zheng, Z. N. Chen, and C.-W. Qiu, Negative reflection and negative refraction in biaxial van der Waals materials, *Nano Letters* **22**, 5607–5614 (2022).
- [13] B. Gérardin, J. Laurent, F. Legrand, C. Prada, and A. Aubry, Negative reflection of elastic guided waves in chaotic and random scattering media, *Scientific Reports* **9**, 10.1038/s41598-019-38480-3 (2019).
- [14] S. Bang, S. So, and J. Rho, Realization of broadband negative refraction in visible range using vertically stacked hyperbolic metamaterials, *Scientific Reports* **9**, 10.1038/s41598-019-50434-3 (2019).
- [15] Z. Jaksic, N. Dalarsson, and M. Maksimovic, Negative refractive index metamaterials: Principles and applications, *Microwave Review* **12** (2006).
- [16] S. Zhang, Y.-S. Park, J. Li, X. Lu, W. Zhang, and X. Zhang, Negative refractive index in chiral metamaterials, *Physical Review Letters* **102**, 10.1103/physrevlett.102.023901 (2009).
- [17] S.-K. Kim, S. Choi, K.-S. Lee, D.-S. Han, D.-E. Jung, and Y.-S. Choi, Negative refraction of dipole-exchange spin waves through a magnetic twin interface in restricted geometry, *Applied Physics Letters* **92** (2008).
- [18] T. Hioki, Y. Hashimoto, and E. Saitoh, Bi-reflection of spin waves, *Communications Physics* **3**, 188 (2020).
- [19] R. Fleury, D. L. Sounas, and A. Alu, Negative refraction and planar focusing based on parity-time symmetric metasurfaces, *Physical Review Letters* **113**, 023903 (2014).
- [20] B. Liu, B. Ren, J. Zhao, X. Xu, Y. Feng, W. Zhao, and Y. Jiang, Experimental realization of all-angle negative refraction in acoustic gradient metasurface, *Applied Physics Letters* **111** (2017).
- [21] S. Mieszczak, O. Busel, P. Gruszecki, A. N. Kuchko, J. W. Klos, and M. Krawczyk, Anomalous refraction of spin waves as a way to guide signals in curved magnonic multimode waveguides, *Physical Review Applied* **13**, 054038 (2020).
- [22] M. Zelent, M. Mailyan, V. Vashistha, P. Gruszecki, O. Gorobets, Y. Gorobets, and M. Krawczyk, Spin wave collimation using a flat metasurface, *Nanoscale* **11**, 9743 (2019).
- [23] X. Wang, J. Ding, B. Zheng, S. An, G. Zhai, and H. Zhang, Simultaneous realization of anomalous reflection and transmission at two frequencies using bi-functional metasurfaces, *Scientific Reports* **8**, 1876 (2018).
- [24] B. Meirbekova, L. Morini, M. Brun, and G. Carta, The strange case of negative reflection, *Applied Physics Letters* **123** (2023).
- [25] S. Liu, T. Jun Cui, A. Noor, Z. Tao, H. Chi Zhang, G. Dong Bai, Y. Yang, and X. Yang Zhou, Negative reflection and negative surface wave conversion from obliquely incident electromagnetic waves, *Light: Science & Applications* **7**, 18008 (2018).
- [26] G. Álvarez-Pérez, J. Duan, J. Taboada-Gutiérrez, Q. Ou, E. Nikulina, S. Liu, J. H. Edgar, Q. Bao, V. Giannini, R. Hillenbrand, *et al.*, Negative reflection of nanoscale-confined polaritons in a low-loss natural medium, *Science Advances* **8**, eabp8486 (2022).
- [27] Y. S. Dadoenkova, I. A. Glukhov, S. G. Moiseev, and F. F. Bentivegna, Non-specular reflection of a narrow spatially phase-modulated gaussian beam, *JOSA A* **39**, 2073 (2022).
- [28] D. D. Stancil and A. Prabhakar, *Spin Waves: Theory and Applications* (Springer, Boston, MA, 2009).
- [29] A. Hubert and R. Schäfer, *Magnetic domains: the analysis of magnetic microstructures* (Springer Science & Business Media, 2008).
- [30] S. Kumar Mishra, H. Prasanth Perumal, and J. Mohanty, Engineering perpendicular magnetic anisotropy and Dzyaloshinskii-Moriya interaction in Gd-Fe thin films for spintronics applications, *Journal of Applied Physics* **136**, 10.1063/5.0244024 (2024).
- [31] L. Fallarino, A. Oelschlägel, J. Arregi, A. Bashkatov, F. Samad, B. Böhm, K. Chesnel, and O. Hellwig, Control

- of domain structure and magnetization reversal in thick Co/Pt multilayers, *Physical Review B* **99**, 024431 (2019).
- [32] N. Vukadinovic, M. Labruno, D. Pain, *et al.*, Magnetic excitations in a weak-stripe-domain structure: A 2D dynamic micromagnetic approach, *Physical Review Letters* **85**, 2817 (2000).
- [33] S. Mondal, A. Talapatra, J. Arout Chelvane, J. R. Mohanty, and A. Barman, Role of magnetic anisotropy in the ultrafast magnetization dynamics of Gd-Fe thin films of different thicknesses, *Phys. Rev. B* **100**, 054436 (2019).
- [34] M. Grassi, M. Geilen, K. A. Oukaci, Y. Henry, D. Lacour, D. Stoeffler, M. Hehn, P. Pirro, and M. Bailleul, Higgs and Goldstone spin-wave modes in striped magnetic texture, *Phys. Rev. B* **105**, 094444 (2022).
- [35] L. M. Alvarez-Prado, Control of dynamics in weak PMA magnets, *Magnetochemistry* **7**, 43 (2021).
- [36] S. Janardhanan, M. Krawczyk, and A. Trzaskowska, Spin-wave dynamics in ultra-thin ferromagnetic films, patterned, and non-patterned, in *Nanomagnets as Dynamical Systems: Physics and Applications*, edited by S. Bandyopadhyay and A. Barman (Springer Nature Switzerland, Cham, 2024) pp. 33–69.
- [37] C. Banerjee, P. Gruszecki, J. W. Klos, O. Hellwig, M. Krawczyk, and A. Barman, Magnonic band structure in a Co/Pd stripe domain system investigated by Brillouin light scattering and micromagnetic simulations, *Physical Review B* **96**, 024421 (2017).
- [38] J. Kisielewski, P. Gruszecki, M. Krawczyk, V. Zablotskii, and A. Maziewski, Between waves and patterns: Spin wave freezing in films with Dzyaloshinskii-Moriya interaction, *Physical Review B* **107**, 134416 (2023).
- [39] M. Bailleul, D. Olligs, and C. Fermon, Micromagnetic phase transitions and spin wave excitations in a ferromagnetic stripe, *Physical review letters* **91**, 137204 (2003).
- [40] G. Leaf, H. Kaper, M. Yan, V. Novosad, P. Vavassori, R. E. Camley, and M. Grimsditch, Dynamic origin of stripe domains, *Phys. Rev. Lett.* **96**, 017201 (2006).
- [41] B. Kalinikos and A. Slavin, Theory of dipole-exchange spin wave spectrum for ferromagnetic films with mixed exchange boundary conditions, *Journal of Physics C: Solid State Physics* **19**, 7013 (1986).
- [42] P. Gruszecki, Y. S. Dadoenkova, N. Dadoenkova, I. Lyubchanskii, J. Romero-Vivas, K. Guslienko, and M. Krawczyk, Influence of magnetic surface anisotropy on spin wave reflection from the edge of ferromagnetic film, *Physical Review B* **92**, 054427 (2015).
- [43] E. M. Lifshitz and L. P. Pitaevskii, *Statistical physics: theory of the condensed state*, Vol. 9 (Butterworth-Heinemann, 1980).
- [44] A. Vansteenkiste, J. Leliaert, M. Dvornik, M. Helsen, F. Garcia-Sanchez, and B. Van Waeyenberge, The design and verification of mumax3, *AIP advances* **4** (2014).
- [45] S. O. Demokritov, V. E. Demidov, O. Dzyapko, G. A. Melkov, A. A. Serga, B. Hillebrands, and A. N. Slavin, Bose–Einstein condensation of quasi-equilibrium magnons at room temperature under pumping, *Nature* **443**, 430 (2006).
- [46] J. Rychły, J. W. Klos, and M. Krawczyk, Spin wave damping in periodic and quasiperiodic magnonic structures, *Journal of Physics D: Applied Physics* **49**, 175001 (2016).
- [47] K. Szulc, S. Tacchi, A. Hierro-Rodríguez, J. Díaz, P. Gruszecki, P. Graczyk, C. Quirós, D. Markó, J. I. Martín, M. Vélez, D. S. Schmool, G. Carlotti, M. Krawczyk, and L. M. Álvarez Prado, Reconfigurable magnonic crystals based on imprinted magnetization textures in hard and soft dipolar-coupled bilayers, *ACS Nano* **16**, 14168 (2022), PMID: 36043881.
- [48] K. Szulc, J. Kharlan, P. Bondarenko, E. V. Tartakovskaya, and M. Krawczyk, Impact of surface anisotropy on the spin-wave dynamics in a thin ferromagnetic film, *Phys. Rev. B* **109**, 054430 (2024).
- [49] A. K. Dhiman, N. Leśniewski, R. Gieniusz, J. Kisielewski, P. Mazalski, Z. Kurant, M. Matczak, F. Stobiecki, M. Krawczyk, A. Lynnyk, *et al.*, Reconfigurable magnonic crystals: Spin wave propagation in Pt/Co multilayer in saturated and stripe domain phase, *APL Materials* **12** (2024).
- [50] N. Salanskii and M. S. Erukhimov, Physical properties and application of magnetic films (1975).
- [51] P. Grünberg, M. Cottam, W. Vach, C. Mayr, and R. Camley, Brillouin scattering of light by spin waves in thin ferromagnetic films, *Journal of Applied Physics* **53**, 2078 (1982).
- [52] G. Dieterle, J. Förster, H. Stoll, A. Semisalova, S. Finizio, A. Gangwar, M. Weigand, M. Noske, M. Fähnle, I. Bykova, *et al.*, Coherent excitation of heterosymmetric spin waves with ultrashort wavelengths, *Physical Review Letters* **122**, 117202 (2019).
- [53] C. Trevillian and V. Tyberkevych, Formation of chirality in propagating spin waves, *npj Spintronics* **2**, 23 (2024).
- [54] V. Veerakumar and R. Camley, Magnon focusing in thin ferromagnetic films, *Physical Review B—Condensed Matter and Materials Physics* **74**, 214401 (2006).
- [55] J.-V. Kim, R. L. Stamps, and R. E. Camley, Spin wave power flow and caustics in ultrathin ferromagnets with the Dzyaloshinskii-Moriya interaction, *Physical Review Letters* **117**, 197204 (2016).

END MATER

Appendix A: Torque components—As described in the main part of the manuscript, Eq. (1) can be expressed in terms of torques as

$$[\partial_t m_x, \partial_t m_z] = \boldsymbol{\tau}^{\text{eff}} = [\tau_x^{\text{eff}}, \tau_z^{\text{eff}}], \quad (\text{A1})$$

where the effective torque $\boldsymbol{\tau}^{\text{eff}}$ consists of multiple contributions: $\boldsymbol{\tau}^{\text{eff}} = \boldsymbol{\tau}^0 + \boldsymbol{\tau}^{\text{ex}} + \boldsymbol{\tau}^{\text{d}} + \boldsymbol{\tau}^{\text{PMA}}$. These terms correspond to torques originating from the external (Zeeman) field, exchange interactions, dipolar interactions, and PMA, respectively.

For a spin wave propagating perpendicular to the bias magnetic field (DE configuration), the individual torque components can be written as:

$$\boldsymbol{\tau}^0 = |\gamma| \mu_0 M_s [(H_0/M_s)m_z, -(H_0/M_s)m_x] \quad (\text{A2})$$

$$\boldsymbol{\tau}^{\text{d}} = |\gamma| \mu_0 M_s [(1 - \xi(kd))m_z, -\xi(kd)m_x] \quad (\text{A3})$$

$$\boldsymbol{\tau}^{\text{ex}} = |\gamma| \mu_0 M_s l_{\text{ex}}^2 k^2 [m_z, -m_x] \quad (\text{A4})$$

$$\boldsymbol{\tau}^{\text{PMA}} = |\gamma| \mu_0 M_s [-Qm_z, 0]. \quad (\text{A5})$$

Appendix B. : Dispersion relation—Assuming harmonic time dependence for m_x and m_z ($m_x, m_z \propto e^{-i\omega t}$), the dispersion relation of SWs can also be derived from Eq. (1).

$$\omega = \sqrt{\omega_x \omega_z}, \quad (\text{A6})$$

where

$$\omega_x = |\gamma| \mu_0 M_s (H/M_s + l_{\text{ex}}^2 k^2 + h_z^{\text{d}} - Q) \quad (\text{A7})$$

$$\omega_z = |\gamma| \mu_0 M_s (H/M_s + l_{\text{ex}}^2 k^2 + h_x^{\text{d}}). \quad (\text{A8})$$

One may notice that ω_x and ω_z are proportional to the x - and z -components of the effective torque acting on magnetization.

Appendix C: Example isofrequency contours—We highlight the presence of intriguingly shaped IFCs in thin films with PMA. The anisotropic dispersion relation of SWs in such structures enables the existence of IFCs difficult or impossible to obtain in other uniform systems. Fig. A1 presents the IFCs for 6.1 GHz, 7.7 GHz, 8.3 GHz, 8.5 GHz, 11 GHz, 13 GHz, 16 GHz and 17 GHz. The unique shape of the contours may allow for further investigation of specular and refractive phenomena in thin films with PMA. An animation showing the smooth

change of the IFC along with the frequency has been posted as an additional video to SM.

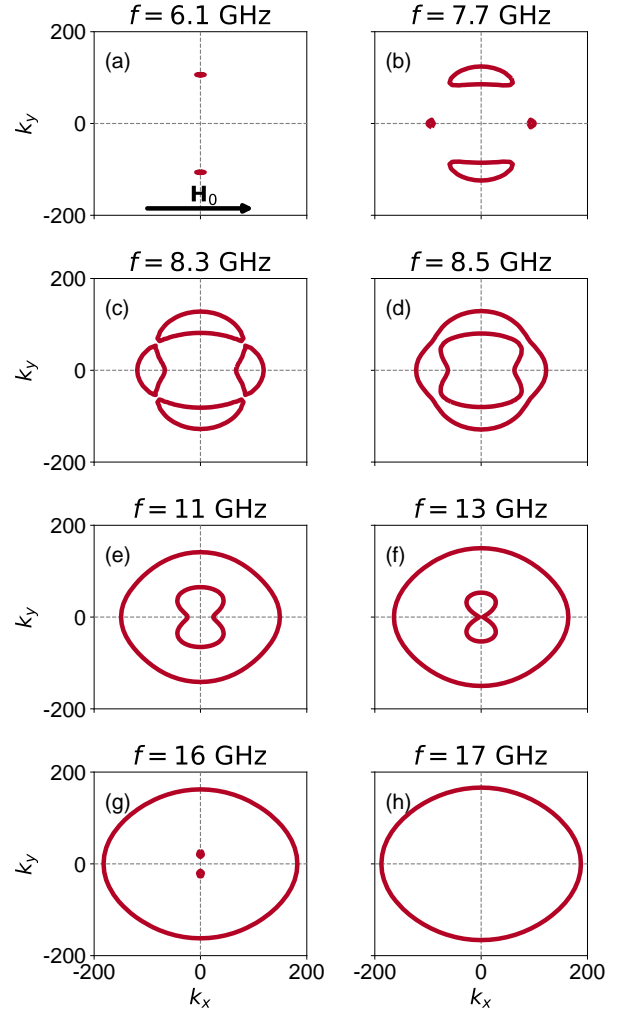


FIG. A1. IFCs extracted from the dispersion relation presented in Fig.3 of the main manuscript for (a) 6.1 GHz, (b) 7.7 GHz, (c) 8.3 GHz, (d) 8.5 GHz, (e) 11 GHz, (f) 13 GHz, (g) 16 GHz, and (h) 17 GHz calculated for SWs in a thin film of thickness $z = 20$ nm. The arrow in (a) shows the direction of the external magnetic field H_0 in all the subsequent plots.